EPJ Web of Conferences **371**, 01004 (2026) https://doi.org/10.1051/epjconf/202637101004
AMT'2026

A thermally robust gradient-based finite-difference scheme for multicomponent compressible reacting flows

Samir El Oteby[1] and *Radouan* Boukharfane[1,*]

[1]College of Computing, Mohammed VI Polytechnic University (UM6P), Benguerir, Morocco

Abstract. We develop a high-order gradient-based reconstruction method for multispecies, chemically reacting compressible flows with temperature-dependent thermodynamics. The approach extends Chamarthi's gradient-based reconstruction strategy to thermally perfect mixtures, where all thermochemical and transport properties are evaluated through Cantera. High-order gradients are computed once per time step and reused for inviscid, viscous, and limiting operations, reducing the cost of multicomponent diffusion and heat-transfer evaluations while preserving accuracy. Shock robustness is ensured through a monotonicity-preserving limiter formulated in characteristic space. The resulting scheme delivers high-order accuracy in smooth regions and sharp, stable resolution of shocks and material interfaces. Benchmark tests—including viscous shock tubes, double Mach reflection, and shock–bubble interaction—demonstrate reduced dissipation and lower computational cost compared with WENO-type schemes.

1 Introduction

High-fidelity simulations of compressible reacting flows remain central to numerous thermal-science applications, including combustion systems, propulsion devices, high-enthalpy gas dynamics, and energy-conversion technologies [1]. The governing multi-species Navier–Stokes equations strongly couple fluid mechanics, thermodynamics, and chemical kinetics. Their accurate solution requires robust treatment of convection, diffusion, and reaction terms [2]. A persistent challenge is computing spatial gradients with sufficient accuracy to predict heat fluxes, species diffusion, vorticity dynamics, and thermodynamic nonequilibrium. In this context, gradient-based reconstruction strategies offer attractive opportunities for enhancing both accuracy and computational efficiency.

Chamarthi [3] introduced a gradient-sharing approach where high-order gradients are computed once and consistently reused for discretizing both inviscid and viscous fluxes. The method demonstrated improved spectral properties, reduced numerical dissipation, and strong high-frequency damping—yielding more accurate viscous-flow solutions and enhanced stability near discontinuities. However, this pioneering work assumed calorically perfect gases, where thermodynamic properties such as C_p, C_v, and γ are constant. This assumption rarely holds in thermal-science applications, where temperature-dependent thermodynamics and multi-species effects are fundamental to accurate prediction.

*e-mail: radouan.boukharfane@um6p.ma

In real reacting systems, strong temperature gradients and chemical composition variations cause significant variations in specific heat capacities and transport properties. These variations directly affect enthalpy transport, heat-release rates, species diffusion, and the local speed of sound. When conservative schemes couple with non-constant thermodynamic properties, spurious pressure and temperature oscillations emerge near shocks, flame fronts, and material interfaces. Such oscillations originate from non-physical smoothing of the specific heat ratio between neighboring cells. The double-flux method, introduced by Abgrall and later refined by Billet and Abgrall, addresses this by freezing a locally consistent thermodynamic state during flux evaluation. Although now widely adopted for thermally perfect gases, this methodology has not yet been integrated into gradient-based high-order reconstructions of the Chamarthi type.

Thermal-science problems also feature strong discontinuities—shocks, contact surfaces, and flame fronts—requiring specialized shock-capturing strategies. Classical approaches include Godunov-type reconstructions, weighted essentially non-oscillatory (WENO) schemes, and monotonicity-preserving (MP) limiters, which eliminate Gibbs oscillations while maintaining high resolution [4]. Comparative studies demonstrate that MP schemes often exhibit lower dissipation and superior convergence properties for wave-propagation problems.

Motivated by these needs and limitations, the present work extends Chamarthi's gradient-sharing methodology to multispecies, chemically reacting flows with temperature-dependent thermodynamic properties. The key innovation is full consistency with thermally perfect gas mixtures whose thermodynamic functions vary with temperature and composition. This requires careful reconstruction of left and right interface states using high-order gradients of primitive variables and ensuring compatibility with temperature-dependent models of $C_p(T)$, $C_v(T)$, $\gamma(T)$, and enthalpy. To manage computational cost, the framework is implemented in parallel, computing gradients once per time step and sharing them efficiently across inviscid, viscous, and limiting operations. This parallel strategy reduces overhead associated with multi-species diffusion and viscous flux evaluations while preserving high-order accuracy for heat and mass transfer.

2 Governing Equations

The solver integrates the compressible Navier–Stokes equations for a multicomponent, reacting gas mixture in nondimensional conservative form [5–7]. The governing system consists of species mass, momentum, and total energy equations,

$$\partial_t \rho_s + \partial_j(\rho_s u_j) = -\frac{1}{Re_r\, S\, c}\,\partial_j J_{j,s} + \dot{\omega}_s, \tag{1}$$

$$\partial_t(\rho u_i) + \partial_j(\rho u_i u_j) = -\frac{1}{\gamma_r M_r^2}\,\partial_i p + \frac{1}{Re_r}\,\partial_j \tau_{ij}, \tag{2}$$

$$\partial_t(\rho e_t) + \partial_j[(\rho e_t + p)u_j] = \partial_j(u_i \tau_{ij}) + \frac{1}{(\gamma_r - 1)\, Re_r\, Pr\, M_r^2}\,\partial_j q_j. \tag{3}$$

Here ρ is the mixture density, u_i the velocity components, $Y_s = \rho_s/\rho$ the species mass fractions, and e_t the total specific energy. The pressure follows the ideal-gas mixture equation of state $p = \rho R T$, with $R = \sum_s Y_s R_s^*$, while the total energy is $e_t^* = \frac{1}{2}u_i^{*2} + \sum_s Y_s(h_s^*(T^*) - R_s^* T^*)$ using thermochemical polynomials from the NASA–Glenn database. The Newtonian stress tensor is

$$\tau_{ij} = \mu\left(\partial_j u_i + \partial_i u_j - \tfrac{2}{3}\delta_{ij}\partial_k u_k\right),$$

with species viscosities from kinetic theory and mixture viscosity from Wilke's rule. Species diffusion is modeled using the mixture-averaged approximation,

$$J_{j,s} = -\rho D\, \partial_j Y_s, \quad D = \mu/\rho,$$

corresponding to a constant Schmidt number $Sc = 0.5$. The heat flux combines Fourier conduction and enthalpy diffusion,

$$q_j = \lambda\, \partial_j T + \sum_s J_{j,s} h_s, \quad \lambda = \mu c_p,$$

with $Pr = 0.73$. Chemical production rates follow a finite-rate mechanism with reactions of the form $\sum_s \nu'_{s,r} X_s \rightleftharpoons \sum_s \nu''_{s,r} X_s$. The dimensional source term is

$$\dot{\omega}^*_s = M^*_s \sum_{r=1}^{n_r} (\nu''_{s,r} - \nu'_{s,r}) \left[k^*_{f,r} \prod_\ell \left(\frac{\rho^*_\ell}{M^*_\ell} \right)^{\nu'_{\ell,r}} - k^*_{b,r} \prod_\ell \left(\frac{\rho^*_\ell}{M^*_\ell} \right)^{\nu''_{\ell,r}} \right],$$

where the forward rates satisfy Arrhenius laws $k^*_{f,r} = A^*_r (T^*)^{\alpha_r} \exp(-\Theta^*_r / T^*)$ and the backward rates are obtained either from an Arrhenius form or from equilibrium constants. The nondimensional source term is written as $\dot{\omega}_s = \frac{\dot{\omega}^*_s}{\rho^*_r u^*_r / L^*_r}$..

All thermodynamic properties, transport coefficients, and chemical source terms are evaluated using the Cantera library [8]. Cantera provides temperature-dependent specific heats, enthalpies, viscosities, thermal conductivities, and diffusion coefficients for multicomponent mixtures, as well as finite-rate chemical kinetics based on detailed or reduced mechanisms. This ensures full consistency with thermally perfect gas behavior, enables accurate coupling between heat release, species diffusion, and flow dynamics, and greatly simplifies integration of complex chemistry in high-order compressible flow simulations.

3 Spatial discretization

3.1 Viscous fluxes

The viscous fluxes for the multicomponent reacting Navier–Stokes equations are evaluated at cell interfaces using a gradient-based formulation consistent with the reconstruction strategy employed for the inviscid terms. In one dimension, the viscous interface flux $\hat{\mathbf{F}}^v_{i+1/2}$ depends on the velocity and temperature gradients, which are reconstructed at $x_{i+1/2}$ using Nishikawa's α-damping formulation to avoid odd–even decoupling and to ensure a consistent discretization of diffusive terms [9]. The interface gradients are obtained from the average of cell-centered gradients supplemented with a damping term proportional to the jump between left and right reconstructed states:

$$\left(\frac{\partial u}{\partial x} \right)_{i+1/2} = \frac{1}{2} \left(u'_i + u'_{i+1} \right) + \frac{\alpha}{2\Delta x} \left(u^R_{i+1/2} - u^L_{i+1/2} \right), \qquad u^{L,R}_{i+1/2} = \hat{u}_{i,i+1} \pm \frac{\Delta x}{2} u'_{i,i+1}.$$

The same construction is applied to the temperature gradient for heat flux computation. Cell-centered gradients u'_i and T'_i are computed using either optimized fourth-order compact finite differences or sixth-order explicit central differences, depending on the chosen accuracy level. Once the gradients are available, the viscous stress and conductive heat flux are evaluated at the interface using these reconstructed gradients. This gradient-based viscous discretization ensures consistency with the high-order interface reconstruction used for convective fluxes and enables efficient reuse of multispecies gradients throughout the solver.

3.2 Convective fluxes

The inviscid fluxes of the multispecies reacting Navier–Stokes equations are discretized using a gradient-based interface reconstruction coupled with a Riemann solver. At each cell interface $x_{i+1/2}$, the numerical flux is obtained by the HLLC solver, written generically as

$$\hat{\mathbf{F}}^{c}_{i+1/2} = \mathbf{F}^{\text{Riemann}}(\mathbf{Q}^{L}_{i+1/2}, \mathbf{Q}^{R}_{i+1/2}) = \frac{1}{2}\Big[\mathbf{F}(\mathbf{Q}^{L}_{i+1/2}) + \mathbf{F}(\mathbf{Q}^{R}_{i+1/2})\Big] - \frac{1}{2}\left|\mathbf{A}_{i+1/2}\right|\Big(\mathbf{Q}^{R}_{i+1/2} - \mathbf{Q}^{L}_{i+1/2}\Big),$$

where $\mathbf{Q}^{L,R}$ are the left and right reconstructed conservative states, and $\mathbf{A}_{i+1/2}$ is the inviscid Jacobian of the multispecies Euler system. The reconstruction of $\mathbf{Q}^{L,R}$ is performed using primitive variables $\mathbf{U}$ so that the high-order gradients already computed for the viscous fluxes can be reused. Inside each cell, the primitive field is approximated by a quadratic expansion

$$\mathbf{U}(x) = \hat{\mathbf{U}}_i + \mathbf{U}'_i(x - x_i) + \frac{1}{2}\kappa\,\mathbf{U}''_i\left[(x - x_i)^2 - \frac{\Delta x^2}{12}\right],$$

and evaluation at the interface $x = x_i \pm \Delta x/2$ gives the left and right states

$$\mathbf{U}^{L}_{i+1/2} = \hat{\mathbf{U}}_i + \frac{\Delta x}{2}\mathbf{U}'_i + \frac{\Delta x^2}{12}\mathbf{U}''_i, \qquad \mathbf{U}^{R}_{i+1/2} = \hat{\mathbf{U}}_{i+1} - \frac{\Delta x}{2}\mathbf{U}'_{i+1} + \frac{\Delta x^2}{12}\mathbf{U}''_{i+1},$$

with $\kappa = 1/3$ as in the standard compact reconstruction. The first derivatives $\mathbf{U}'_i$ are those already computed and shared for the viscous discretization, using either optimized fourth-order compact schemes or sixth-order explicit central differences. The second derivatives $\mathbf{U}''_i$ are obtained directly from these first derivatives using the relation

$$\mathbf{U}''_i = \frac{2}{\Delta x^2}\left(\hat{\mathbf{U}}_{i+1} - 2\hat{\mathbf{U}}_i + \hat{\mathbf{U}}_{i-1}\right) - \frac{1}{2\Delta x}\left(\mathbf{U}'_{i+1} - \mathbf{U}'_{i-1}\right),$$

which avoids additional stencil operations and preserves consistency with the gradients used for viscous terms. Once the interface primitive states are known, they are converted to conservative variables $\mathbf{Q}$ and supplied to the Riemann solver. For multispecies flows, the primitive vector contains the species partial densities, velocity components, and pressure, and the conversion to conservative form uses thermodynamic properties obtained from Cantera, ensuring full consistency with the local mixture composition, temperature-dependent heat capacities, and multispecies equation of state. This gradient-based reconstruction (GRB) approach provides high-order accuracy, preserves the coupling between flow and thermochemistry, and enables reuse of the same high-order gradients throughout both the inviscid and viscous discretizations.

3.3 Shock-capturing approach

To stabilize the high-order gradient-based reconstruction in the presence of shocks, contact discontinuities, and material interfaces, the inviscid fluxes are supplemented with a monotonicity-preserving (MP) nonlinear limiting procedure. The MP limiter of Suresh and Huynh is applied to the left and right interface states reconstructed by the GRB scheme described previously. For each interface $x_{i+1/2}$, the unlimited left state is first obtained via the quadratic gradient-based reconstruction:

$$\mathbf{U}^{L,GRB}_{i+1/2} = \hat{\mathbf{U}}_i + \frac{\Delta x}{2}\mathbf{U}'_i + \frac{\Delta x^2}{12}\mathbf{U}''_i,$$

where both $\mathbf{U}_i'$ and $\mathbf{U}_i''$ are the high-order gradients already computed for the viscous fluxes. A smoothness check is then performed by comparing $\mathbf{U}_{i+1/2}^{L,GRB}$ with the admissible interval defined by the cell-centered values $\hat{\mathbf{U}}_i$, $\hat{\mathbf{U}}_{i\pm1}$ and the MP predictor:

$$\mathbf{U}^{MP} = \hat{\mathbf{U}}_i + \texttt{minmod}\Big(\hat{\mathbf{U}}_{i+1} - \hat{\mathbf{U}}_i,\, \beta(\hat{\mathbf{U}}_i - \hat{\mathbf{U}}_{i-1})\Big),$$

with $\beta = 7$ as in standard MP practice. If the high-order reconstruction lies within these bounds, no limiting is applied and the GRB interface value is retained. Otherwise, the limiter constructs bounded interface values using local curvature information. In the present solver, this curvature is evaluated using the same second derivative available from the viscous discretization:

$$d_i = 2(\hat{\mathbf{U}}_{i+1} - 2\hat{\mathbf{U}}_i + \hat{\mathbf{U}}_{i-1}) - \frac{\Delta x}{2}\left(\mathbf{U}'_{i+1} - \mathbf{U}'_{i-1}\right),$$

and a two-point `minmod` curvature at the interface:

$$d_{i+1/2}^{M} = \texttt{minmod}(d_i, d_{i+1}).$$

These quantities define lower and upper admissible interface values, $\mathbf{U}_{i+1/2}^{\min}$ and $\mathbf{U}_{i+1/2}^{\max}$, obtained from MP upwind, midpoint, and local-centered predictors. The limited left interface state is finally computed via

$$\mathbf{U}_{i+1/2}^{L,MP} = \mathbf{U}_{i+1/2}^{L,GRB} + \texttt{minmod}\Big(\mathbf{U}_{i+1/2}^{\min} - \mathbf{U}_{i+1/2}^{L,GRB},\, \mathbf{U}_{i+1/2}^{\max} - \mathbf{U}_{i+1/2}^{L,GRB}\Big),$$

and an analogous expression provides the right interface state. Because the Euler equations form a coupled hyperbolic system, the entire limiting procedure is performed in characteristic space: the primitive variables and their gradients are projected using Roe-averaged eigenvectors, limited componentwise, and mapped back to physical space. This ensures clean separation of waves and mitigates cross-variable contamination near discontinuities. The resulting nonlinear schemes, based on either explicit or compact gradient evaluations, provide sharp and stable shock resolution while preserving the high-order accuracy of the gradient-based reconstruction in smooth regions. Importantly, all nonlinear smoothness indicators reuse the same high-order gradients and curvatures employed in the viscous discretization, ensuring full consistency and computational efficiency.

4 Results and discussion

4.1 Monodimensional shock tube

This test case compares the computational cost of the GRB algorithm with several widely used schemes, such as WENO5-JS, using a two-species (N_2/O_2) mixture. The simulation is performed in a viscous setting to evaluate the impact of reusing velocity gradients throughout the algorithm. A discontinuity separating two thermodynamic states is initially positioned at the midpoint of the tube ($x = 0.5$). The initial conditions are:

$$(\rho, u, v, w, p) = \begin{cases} (1, 0, 0, 0, 1), & 0 \le x < 0.5, \\ (0.125, 0, 0, 0, 0.1), & 0.5 \le x \le 1. \end{cases}$$

The case is solved on a computational domain $x \in [0, 1]$ using $N = 200$ uniformly spaced grid points, advanced in time up to $t = 0.2$. The GRB scheme successfully captures both the discontinuity and the shock wave. As shown in Table 1, the GRB scheme requires less computational time compared to competing methods across all grid resolutions.

Table 1. Wall-clock computational time in seconds for different WENO-type schemes and the GRB method.

Grid N_x	GRB	TENO5-Z	WENO5-JS	WENO5-M	WENO5-Z
200	0.39	0.57	0.47	0.48	0.43
400	1.43	2.12	1.68	1.80	1.63
600	3.06	4.73	3.78	4.03	3.67
800	5.50	8.36	6.95	7.11	6.65
1000	8.71	13.23	10.59	11.50	10.13
1200	12.87	18.97	15.20	16.77	14.78
1400	17.58	25.81	20.74	22.98	19.80
1600	22.92	33.87	26.76	30.07	25.80

4.2 Double Mach reflection

This test case is initialized with two uniform states of an N_2/O_2 mixture separated by an oblique shock inclined at 30°. At $t = 0$, the shock intersects the lower boundary at $(x_s, y_s) = (1/6, 0)$, and its initial position is described by

$$y = \sqrt{3}\left(x - \frac{1}{6}\right).$$

The pre-shock (left) state, corresponding to a Mach-10 inflow for $\gamma = 1.4$, is

$$(\rho, u, v, p)_L = (8,\ 8.25\cos 30^\circ,\ -8.25\sin 30^\circ,\ 116.5)\,,$$

while the post-shock (right) state is

$$(\rho, u, v, p)_R = (1.4,\ 0,\ 0,\ 1).$$

The initial condition is imposed in piecewise form as

$$(\rho, u, v, p) = \begin{cases} (8,\ 8.25\cos 30^\circ,\ -8.25\sin 30^\circ,\ 116.5)\,, & x < \dfrac{1}{6} + \dfrac{y}{\tan 60^\circ}, \\ (1.4,\ 0,\ 0,\ 1)\,, & x > \dfrac{1}{6} + \dfrac{y}{\tan 60^\circ}. \end{cases}$$

This setup ensures a clean evolution of the incident and reflected shocks, the Mach stem, and the slip line, while preventing any upper-boundary artifacts. The simulation is carried on a 900×350 grid over the domain $[0, 4] \times [0, 1]$ using a constant CFL number of 0.2, and the solution is advanced to $t = 0.2$. Because the Euler equations contain no physical viscosity, the formation of Kelvin–Helmholtz vortices along the slip line and the development of the near-wall jet directly reflect the numerical dissipation of each method. As shown in Fig. 1, the GRB scheme captures more vortices and produces a stronger near-wall jet than WENO5-JS, indicating less dissipative behavior.

4.3 Shock–Bubble interaction

In this test case, we examine the interaction between a planar Mach 1.22 shock wave and a helium bubble. For simplicity, both air and helium are treated as ideal gases. The bubble, having an initial radius of 0.5, is positioned at $(x, y) = (3.5, 0.89)$ within a computational domain of size $[0,\ 6.5]\times[0,\ 1.78]$. The shock is initially placed at $x = 4.5$. Outflow conditions

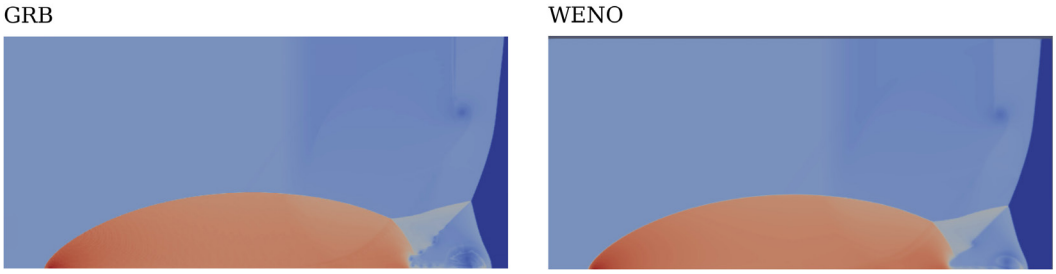

Figure 1. Density profiles at $t = 0.2$ obtained with the GRB and WENO5-JS schemes in the enlarged region around the Mach stem, computed on a 900×350 grid.

are applied on the left boundary, while inflow conditions are imposed on the right, and slip-wall boundary conditions are used along the top and bottom walls. The initial flow states on either side of the shock are determined from Rankine–Hugoniot relations:

$$(\rho, u, v, w, p) = \begin{cases} (1.0,\ 0,\ 0,\ 0,\ 1), & \text{pre-shocked air,} \\ (1.3764,\ -0.3947,\ 0,\ 0,\ 1.5698), & \text{post-shocked air,} \\ (0.1819,\ 0,\ 0,\ 0,\ 1), & \text{helium bubble.} \end{cases}$$

The simulations are performed on a 1300×350 uniform grid, corresponding to $\Delta x = \Delta y = 0.005$, and advanced in time up to $t = 2.0$ s. As illustrated in Fig. 2, the GRB scheme resolves a greater number of fine-scale vortical structures compared to WENO5-JS, again demonstrating the reduced dissipation of the gradient-based approach.

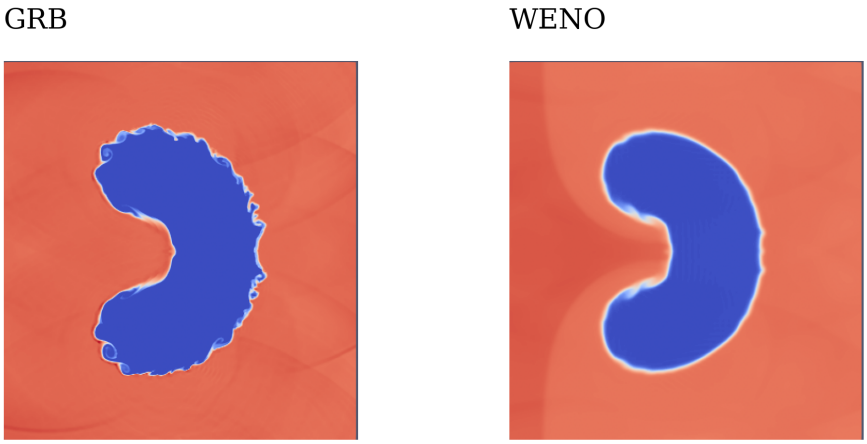

Figure 2. Density plots for GRB and WENO5-JS, at $t = 2.0$ s for the shock–bubble example on a 1300×350 uniform grid.

5 Conclusion

A high-order gradient-based reconstruction framework has been presented for multispecies, chemically reacting flows with temperature-dependent thermodynamic properties. By computing gradients once per time step and reusing them consistently in the inviscid fluxes, viscous terms, and nonlinear limiting procedure, the method achieves both improved accuracy and reduced computational cost. The integration of thermally perfect gas models through Cantera ensures full consistency between thermochemistry, transport, and fluid dynamics, while the monotonicity-preserving limiter formulated in characteristic space provides robust shock resolution.

Demonstrations on canonical test cases show that the proposed scheme captures fine-scale flow structures with significantly less dissipation than classical WENO-type methods and delivers clear efficiency gains across a range of grid resolutions. These results highlight the potential of gradient-sharing strategies as an effective tool for high-fidelity simulation of thermally driven, multicomponent compressible flows. Future work will explore application to chemically reacting flows with detailed kinetics and three-dimensional simulations on parallel architectures.

References

[1] R. Boukharfane, Ph.D. thesis, ISAE-ENSMA, Poitiers (2018)

[2] T. Poinsot, D. Veynante, Theoretical and numerical combustion (RT Edwards, Inc., 2005)

[3] A.S. Chamarthi, Gradient based reconstruction: Inviscid and viscous flux discretizations, shock capturing, and its application to single and multicomponent flows, Computers & Fluids **250**, 105706 (2023).

[4] R. Bozorgpour, H.M. Darian, Recent advancements in fluid flow simulation using the WENO scheme: A comprehensive review, Journal of Nonlinear Mathematical Physics **32**, 14 (2025).

[5] S. Baaziz, R. Boukharfane, Large eddy simulation of highly underexpanded sonic jets from elliptical nozzles, Physics of Fluids **36** (2024).

[6] R. Boukharfane, A. Er-raiy, M. Elkarii, M. Parsani, A direct numerical simulation study of skewed three-dimensional spatially evolving compressible mixing layer, Physics of Fluids **33** (2021).

[7] R. Boukharfane, Highly resolved numerical simulation of pure and blended fuel sonic jets in a Mach 2 crossflow, Engineering Applications of Computational Fluid Mechanics **19**, 2538815 (2025).

[8] D.G. Goodwin, Cantera C++ user's guide, California Institute of Technology **32**, 358 (2002).

[9] H. Nishikawa, Two ways to extend diffusion schemes to Navier-Stokes schemes: Gradient formula or upwind flux, in *20th AIAA Computational Fluid Dynamics Conference* (2011), p. 3044